

First calculation of the $\gamma\gamma$ -decay width of a nuclear 2_1^+ state: The case of ^{48}Ca

A. P. Severyukhin^{1,2}, N. N. Arsenyev,¹ and N. Pietralla³

¹*Bogoliubov Laboratory of Theoretical Physics, Joint Institute for Nuclear Research, 141980 Dubna, Moscow Region, Russia*

²*Dubna State University, 141982 Dubna, Moscow Region, Russia*

³*Institut für Kernphysik, Technische Universität Darmstadt, 64289 Darmstadt, Germany*



(Received 20 July 2020; revised 1 June 2021; accepted 22 July 2021; published 5 August 2021)

The competitive double- γ decay of the 2_1^+ state of an even-even spherical nucleus is studied for the first time. The coupling of one-, two-, and three-phonon terms in the wave functions of excited states is taken into account within the microscopic model based on the Skyrme energy density functional. The approach enables one to perform the calculations in very large configurational spaces. We estimate the generalized electric dipole polarizabilities involved in the $\gamma\gamma/\gamma$ decay process and make a prediction for the branching ratio of the competitive $\gamma\gamma$ -decay relative to its single γ -decay calculated to be 3×10^{-8} for the case of ^{48}Ca .

DOI: [10.1103/PhysRevC.104.024310](https://doi.org/10.1103/PhysRevC.104.024310)

I. INTRODUCTION

In Ref. [1], the $\gamma\gamma$ decay of a nuclear transition in competition with an allowed γ decay has been discovered. This is the observation of the $\gamma\gamma$ decay of the first excited $J^\pi = 11/2^-$ state of ^{137}Ba directly competing with an allowed γ decay to the $J^\pi = 3/2^+$ ground state. The branching ratio of the competitive $\gamma\gamma$ decay of the $11/2^-$ isomer of the odd-even nucleus ^{137}Ba to the ground state relative to its single γ decay was determined to be $(2.05 \pm 0.37) \times 10^{-6}$. This discovery has very recently been confirmed and the data were made more precise, in particular with respect to the contributing multipolarities [2].

The $\gamma\gamma$ -decay reactions are formally analogous to neutrinoless double- β decay ($0\nu\beta\beta$ -decay) processes where in the latter two β particles and in the former two γ -quanta appear in the final state and share the total transition energy. Indeed, $\gamma\gamma$ -decay processes have first theoretically been postulated and studied by Maria Göppert in her Ph.D. thesis [3] with Max Born in Göttingen, even before discussing $\beta\beta$ -decay processes. While various predictions for the $0\nu\beta\beta$ -nuclear matrix elements are on the market, e.g., from Refs. [4–6], there is no way to test the accuracy of the theoretical calculations without a firm measurement of the $0\nu\beta\beta$ -decay rate. The $2\nu\beta\beta$ -decay rate is a useful tool for testing the accuracy of calculations that try to predict the $0\nu\beta\beta$ rate, but it is certainly not enough for making predictions for the $0\nu\beta\beta$ rates [5]. Although $\beta\beta$ -decay processes are nuclear reactions of second order in the electroweak interaction, it is surprising to find that even less data exist for nuclear decay reactions that proceed in second order in the electromagnetic interaction where two γ quanta are simultaneously emitted in a single quantum transition from one quantum state to another. Up to recently, $\gamma\gamma$ -decay reactions in the even-even nuclei were known only in three particular cases, ^{16}O [7,8] and ^{40}Ca and ^{90}Zr [9,10], where the first excited states of these even-even nuclei have spin and

parity quantum numbers 0^+ and a single- γ decay is strictly forbidden by helicity conservation.

The $E1E1$ transition from the $2s$ to $1s$ level in the H atom and low- Z H-like ions is a proverbial example for atomic systems. It is the most probable decay mode and therefore defines the lifetime of the $2s$ level. The first estimate was obtained by Breit and Teller in Ref. [11]. However, the nuclear $\gamma\gamma$ decay dominated by $E1E1$ contribution has not yet been found.

In this paper, we report on the more general situation, in which the $\gamma\gamma$ decay of the low-energy quadrupole state occurs in a nuclear transition which could proceed by a single- γ decay in competition.

Using $\hbar = c = 1$, the γ decay width of the 2_1^+ state of even-even nuclei is related to its reduced electric quadrupole transition strength, $B(E2; 2_1^+ \rightarrow 0_{\text{gs}}^+)$, via

$$\Gamma_\gamma = \frac{4\pi}{75} (E_{2_1^+})^5 B(E2; 2_1^+ \rightarrow 0_{\text{gs}}^+). \quad (1)$$

To describe the $\gamma\gamma$ decay between the 2_1^+ and 0_{gs}^+ states, we use a formalism that explicitly relates the electromagnetic interaction up to second order in the electromagnetic operators and two-quantum processes in atomic nuclei [12]. Thus, the $\gamma\gamma$ -decay width can be estimated as

$$\Gamma_{\gamma\gamma'} = \frac{64\pi}{42525} (E_{2_1^+})^7 (\alpha_{E1E1})^2 (1 + \delta), \quad (2)$$

with

$$\alpha_{E1E1} = \sum_i \frac{\langle 0_{\text{gs}}^+ || M(E1) || 1_i^- \rangle \langle 1_i^- || M(E1) || 2_1^+ \rangle}{E_{1_i^-} - 0.5E_{2_1^+}}, \quad (3)$$

$$\delta = \left(\frac{\alpha_{M1M1}}{\alpha_{E1E1}} \right)^2 + \frac{3}{11} 10^{-4} \left(\frac{\alpha_{E2E2}}{\alpha_{E1E1}} \right)^2 (E_{2_1^+})^4 + \dots \quad (4)$$

The $\gamma\gamma$ -decay width is dominated by the $E1E1$ contribution, i.e., $\delta \ll 1$. One may easily confirm this statement in

a two-state scenario by using the $M1$ sum rule. The $M1M1$ component to the $\gamma\gamma/\gamma$ decay of the 2_1^+ state of any nucleus is much smaller than the α_{E1E1} component discussed here in the case of ^{48}Ca , taken as an example.

The doubly magic nucleus ^{48}Ca has provided a crucial testing ground for nuclear theories (see, e.g., Refs. [13,14]). In this connection, the electric dipole polarizability,

$$\alpha_D = \frac{8\pi}{9} \sum_i \frac{\langle 0_{\text{gs}}^+ || M(E1) || 1_i^- \rangle \langle 1_i^- || M(E1) || 0_{\text{gs}}^+ \rangle}{E_{1_i^-}}, \quad (5)$$

is playing an important role; in particular, its value has strong implications in constraining the symmetry energy J including its density dependence and slope parameter L of the nuclear equation of state [15]. The symmetry energy also plays an important role in nuclei, where it contributes to the formation of neutron skins in the presence of a neutron excess. Calculations based on energy density functionals (EDFs) pointed out that J and L can be correlated with isovector collective excitations of the nucleus, such as pygmy dipole resonances (PDRs) [16] and giant dipole resonances (GDRs) [17], thus suggesting that the neutron skin thickness [18], the difference of the neutron and proton root-mean-square radii, could be constrained by studying properties of collective isovector observables at low energy. Since α_D and α_{E1E1} are challenging but in principle accessible observables, it is useful to compare their values. We provide here first information on their relation.

II. FORMALISM

Our tool is the random phase approximation (RPA) with Skyrme EDF. The residual particle-hole interaction is obtained as the second derivative of the energy density functional with respect to the particle density. By means of the standard procedure [19], we obtain the familiar equations of the RPA in the one particle–one hole (1p-1h) configuration space. The eigenvalues of the RPA equations are found numerically as the roots of a relatively simple secular equation within the finite-rank separable approximation (FRSA) [20,21] which allows one to perform the calculations in large configurational spaces. In particular, the cutoff of the discretized continuous part of the single-particle spectra is at the energy of 100 MeV. This is sufficient to exhaust practically all the energy-weighted sum rule within the RPA [21]. Further technical details of the calculations are provided in Appendix A.

Being a linear combination of 1p-1h states, the RPA solutions are treated as quasibosons with quantum numbers $\lambda^\pi: Q_{\lambda\mu i}^+(0)$. The value μ denotes the z projection of the total angular momentum in the laboratory system. Among these solutions, there are one-phonon states corresponding to collective GDRs and pure 1p-1h states. The configurations with various degrees of complexity can be built by combining different one-phonon configurations of fixed quantum number $J^\pi = 1^-$. Taking into account the basic ideas of the quasiparticle-phonon model (QPM) [22], the Hamiltonian is then diagonalized in a space spanned by states composed of one, two, and three RPA phonons. This implies that the rank of the set of linear equations is equal to the number of one-, two-, and three-phonon configurations included in the wave

function,

$$\begin{aligned} \Psi_\nu(JM) = & \left(\sum_i R_i(J\nu) Q_{JM i}^+ + \sum_{\substack{\lambda_1 i_1 \\ \lambda_2 i_2}} P_{\lambda_2 i_2}^{\lambda_1 i_1}(J\nu) [Q_{\lambda_1 i_1}^+ Q_{\lambda_2 i_2}^+]_{JM} \right. \\ & \left. + \sum_{\substack{\lambda_1 i_1 \\ \lambda_2 i_2 \\ \lambda_3 i_3 J'}} T_{J' \lambda_3 i_3}^{\lambda_1 i_1 \lambda_2 i_2}(J\nu) [[Q_{\lambda_1 i_1}^+ Q_{\lambda_2 i_2}^+]_{J'} Q_{\lambda_3 i_3}^+]_{JM} \right) |0\rangle. \end{aligned} \quad (6)$$

Its solution requires computation of the matrix elements of the quasiparticle-phonon interaction [23], $\langle 0 | Q_{Ji} H [Q_{\lambda_1 i_1}^+ Q_{\lambda_2 i_2}^+]_{J'} | 0 \rangle$. The equations of the phonon-phonon coupling (PPC) have the same form as the QPM equations [24,25], but the single-particle spectrum and the parameters of the residual interaction are calculated with the chosen Skyrme EDF without any further adjustments [23]. We consider widely used SLy5 EDF [26], which is adjusted to reproduce the enhancement factor of the Thomas-Reiche-Kuhn (TRK) sum rule $\kappa = 0.25$ and the nuclear matter properties, as well as nuclear charge radii and binding energies of doubly magic nuclei [27]. Also the excitation energy $E_x = 3.832$ MeV and the decay transition strength $B(E2; 2_1^+ \rightarrow 0_{\text{gs}}^+) = 1.71 \pm 0.09$ W.u. of the 2_1^+ state of ^{48}Ca [28] are reasonably well described in the RPA with the same set of parameters, yielding $E_x = 3.19$ MeV and $B(E2) = 1.3$ W.u. [29]. The inclusion of the phonon-phonon coupling plays a minor role in the 2_1^+ state's description. The crucial contribution to the wave function comes from the neutron configuration $\{1f_{7/2}^{-1}, 2p_{3/2}\}$.

In the actual calculations (PPC3), we have included in our model space different multipoles $\lambda^\pi = 1^-, 2^+, 3^-,$ and 4^+ . Tentative estimates for the position of the resonance centroid E_c and the spreading width Γ are defined by means of the energy-weighted moments $m_k = \sum B(E1) E^k$: (i) $E_c = m_1/m_0$ and (ii) $\Gamma = \sqrt{m_2/m_0 - (m_1/m_0)^2}$, taking 92% of the TRK sum rule, i.e., $(1 + \kappa)14.8NZ/A e^2 \text{ fm}^2 \text{ MeV}$. The $E1$ transitions are corrected for the center-of-mass motion; see Appendix B. All one-, two-, and three-phonon configurations with energies up to $E = 27$ MeV are included. The inclusion of high-energy configurations plays a minor role in our calculations. At the same time, the extension of the configurational space to the two- and three-phonon configurations has a strong effect on the low-energy 1^- spectrum, shown in Fig. 1. If we omit the three-phonon configurations, then this calculation is hereafter called PPC2. Further, the PPC2 calculation taking into account the coupling with $[2_1^+]_{\text{RPA}}$ phonon only is named PPC2- 2_1^+ .

III. RESULTS

The photoabsorption cross section in $^{48}\text{Ca}(p, p')$ is measured in the range from 10 to 25 MeV [32]. The general shape of the $E1$ strength distribution obtained in the PPC3 calculation is rather close to that observed in experiment; see Fig. 2(a). The calculated integral characteristics of the GDR ($E_c = 19.1$ MeV and $\Gamma = 3.1$ MeV) are in

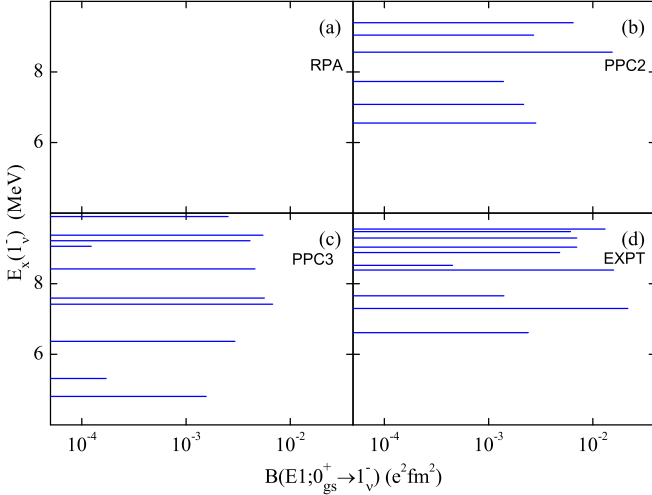


FIG. 1. The phonon-phonon coupling effect on the $B(E1)$ strength distribution. Experimental data are taken from Ref. [30].

satisfactory agreement with the experimental data on ^{48}Ca [32]. The inclusion of the PPC effects yields a noticeable redistribution of the GDR strength in comparison with the RPA results. In Ref. [29], the role of the coupling of the one- and

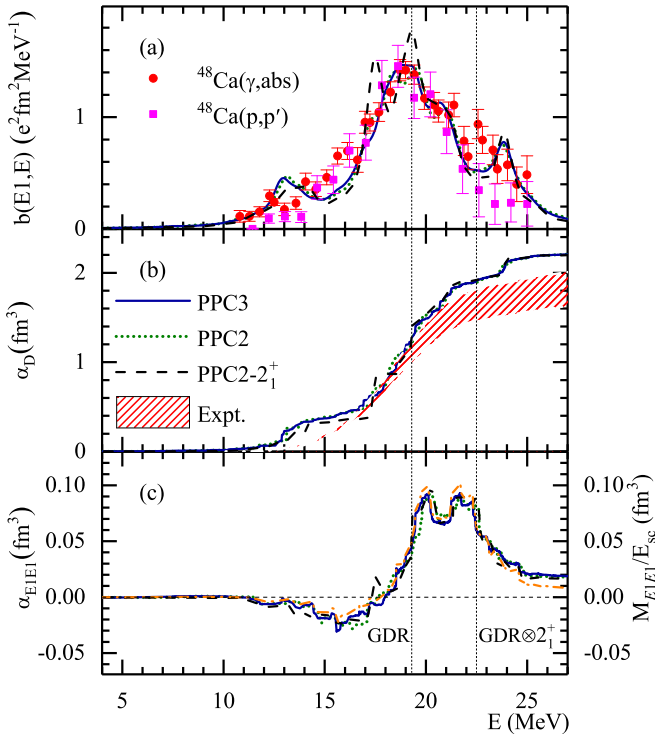


FIG. 2. (a) The $B(E1)$ strength distribution. The smoothing parameter 1 MeV is used for the strength distribution described by the Lorentzian function. Experimental data are taken from Refs. [31,32]. The dashed, dotted, and solid lines correspond to the PPC2- 2_1^+ , PPC2, and PPC3 calculations, respectively. (b) Running sum of the polarizability α_D . The shaded area indicates experimental upper and lower limits [32]. (c) Running sum of the generalized polarizability α_{E1E1} and the value M_{E1E1}/E_{sc} (the dash-dotted line).

two-phonon configurations on the $E1$ strength-distribution calculations with the SLy5 EDF has been examined.

The electric dipole polarizability of $\alpha_D = 1.73 \pm 0.18 \text{ fm}^3$ has been measured in the range from 10 to 25 MeV in Ref. [32]. Running sums of the α_D value for ^{48}Ca in the energy region below 27 MeV are given in Fig. 2(b). The steep rise in the theoretical band around 19 MeV indicates that the position of the GDR peak is consistent with the experimental centroid. The fact that the slope is well reproduced indicates that the spreading is well described. Inclusion of PPC does not change the value of α_D obtained by integrating the $E1$ strength up to 25 MeV: $\alpha_D = 2.16 \text{ fm}^3$ in the case of the PPC2 and $\alpha_D = 2.17 \text{ fm}^3$ in the PPC3. The contribution $[0.0101 \pm 0.0006 \text{ fm}^3]$ found experimentally below 10 MeV is negligible. Our calculations predict, below 10 MeV, $\alpha_D = 0.015 \text{ fm}^3$ and 0.017 fm^3 within PPC2 and PPC3, respectively. These values are indeed negligible, as for the experimental case. A similar conclusion was made in Ref. [33], where the EDFs SGII and SLy4 were used. Thus, the main contribution to the α_D polarizability comes from the one-phonon configurations.

The calculated value for the α_{E1E1} matrix element for the $\gamma\gamma$ decay is 0.018 fm^3 within the PPC2 and 0.019 fm^3 in the case of the PPC3 at 1^- energies below 27 MeV. The running sum of α_{E1E1} is very instructive with respect to various energy regions of the 1^- spectrum; see Fig. 2(c). We obtain two regimes: a rapid rise in the energy region $16 < E_x < 20 \text{ MeV}$ and a steep decline in the energy region $22 < E_x < 25 \text{ MeV}$, respectively. In the first energy region, the crucial component to the α_{E1E1} value comes from a coherent contribution of 1^- states in the sum of product of $E1$ matrix elements

$$M_{E1E1} = \sum_i \langle 0_{gs}^+ || M(E1) || 1_i^- \rangle \langle 1_i^- || M(E1) || 2_1^+ \rangle \quad (7)$$

belonging to the GDR; see Fig. 3(a). The running sum for α_{E1E1} decreases at energies above 22 MeV due to a coherent contribution with a negative sign in this energy range; see Fig. 3(b). This implies that the calculated $E1$ matrix elements represent two dominant substructures of the dipole strength distribution; see the dash-dotted line of Fig. 2(c). We study them first in a simple two-state mixing scenario taking into account the GDR and the initial, 2_1^+ , and final, 0_{gs}^+ , states of the generalized polarizability.

We construct a two-state mixing scheme by considering the GDR state, the coupled $\text{GDR} \otimes 2_1^+$ state, and the interaction V between them. The relative phases of amplitudes are opposite in the perturbed states I and II, i.e.,

$$|1_I^-\rangle = \alpha |\text{GDR}\rangle + \beta |\text{GDR} \otimes 2_1^+\rangle, \quad (8)$$

$$|1_{II}^-\rangle = -\beta |\text{GDR}\rangle + \alpha |\text{GDR} \otimes 2_1^+\rangle. \quad (9)$$

The two-state mixing scheme provides the simple expression

$$\frac{\alpha_{E1E1}}{\alpha_D} = \frac{9}{8\pi} \frac{\alpha\beta(E_{II} - E_I)}{\alpha^2 E_{II} + \beta^2 E_I}, \quad (10)$$

in the typical situation where the energies E_{II} and E_I are much larger than $E_x(2_1^+)/2$. Notice that $\alpha_{E1E1}/\alpha_D = 0$ if the basis configurations do not mix. The amplitudes, α and β , can be estimated in the two limiting cases of weak or strong mixing, where either the interaction V is much smaller than

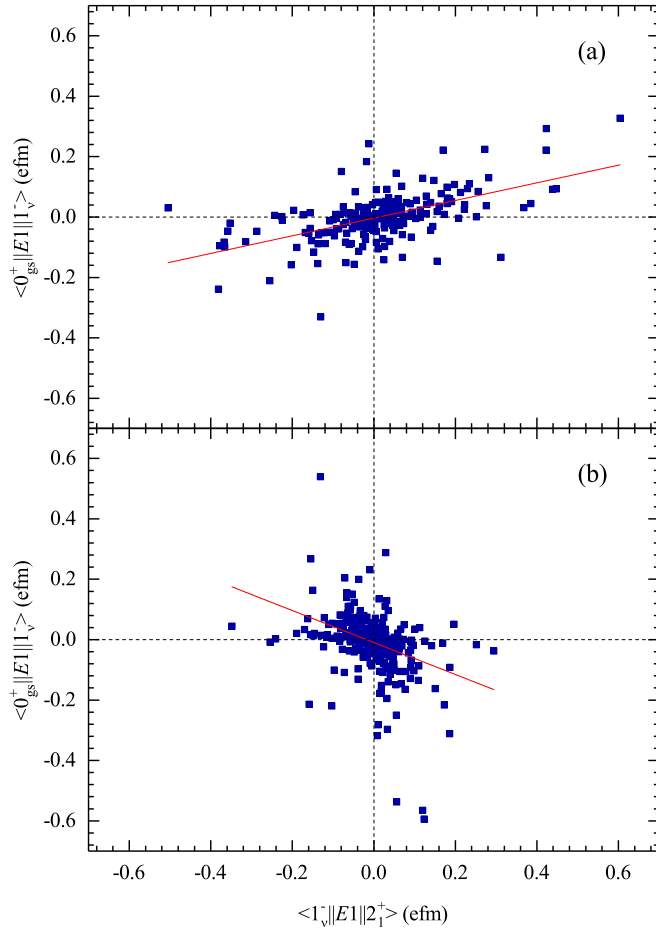


FIG. 3. Reduced matrix elements of $E1$ transitions in the following energy interval: from 16 until 20 MeV (a) and from 22 until 25 MeV (b).

the difference of the unperturbed energies [$\Delta E_u = E_x(2_1^+)$], or the two unperturbed states are degenerate ($\Delta E_u = 0$). For these cases, we obtain

$$\frac{\alpha_{E1E1}}{\alpha_D} = \frac{9}{8\pi} \frac{V}{E_{GDR} + 0.5\Delta E_u}. \quad (11)$$

Figure 2(c) shows that the running sum of α_{E1E1} remains more or less unchanged when comparing the full result with the calculation taking into account the PPC with the $[2_1^+]_{\text{RPA}}$ phonon, only. Therefore, we can simulate the full diagonalization reasonably well by using a two-state mixing [34]; see Fig. 4. The GDR state built on the most collective RPA states, the two-phonon GDR $\otimes 2_1^+$ state, and the interaction

$$V = \frac{1}{\sqrt{N_{1\text{ph}}N_{2\text{ph}}}} \sum_{i=1}^{N_{1\text{ph}}} \sum_{k=1}^{N_{2\text{ph}}} \langle 0 | Q_{1i} H [Q_{21}^+ Q_{1k}^+]_1 | 0 \rangle, \quad (12)$$

between them, have been calculated from the SLy5 EDF.

The two-state model can also help to estimate the value α_{M1M1} of $0.05 \mu_N^2 \text{ MeV}^{-1}$; see Appendix C. The $M1$ transition matrix elements calculated without spin-gyromagnetic quenching factor leads to an upper limit for α_{M1M1} . The $M1M1$ component dominates in the correction δ of Eq. (4): $\delta(M1) = 1.7 \times 10^{-3}$ and $\delta(E2) = 1.9 \times 10^{-7}$. Thus, keeping

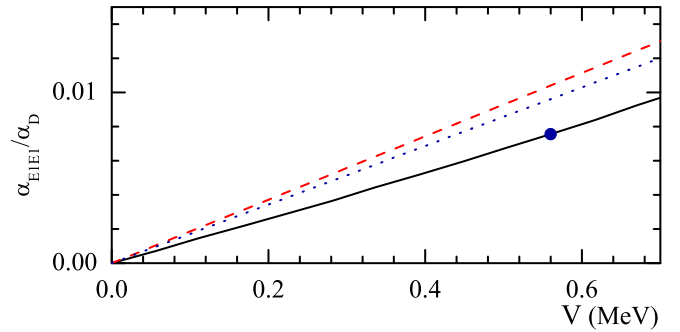


FIG. 4. The ratio between polarizabilities α_D and α_{E1E1} as a function of the mean value V of the matrix elements coupling one- and two-phonon configurations. The solid line corresponds to the PPC2- 2_1^+ calculation taking into account scaling of the quasiparticle-phonon interaction. The results of the two-state model with $\Delta E_u = 0$ and 3.2 MeV are denoted by the dashed line and the dotted line, respectively. The PPC3 calculation of SLy5 is denoted by the circle.

only 1^- virtual states is a satisfactory approximation for the $\gamma\gamma$ decay width. It is worth mentioning that in ^{48}Ca the spin-flip $M1$ resonance having a noncollective structure being dominated by the neutron configuration $\{1f_{7/2}^{-1}, 1f_{5/2}\}$ is a key reference for an interpretation of the quenching phenomenon; see, e.g., Ref. [35].

In total, our PPC3 analysis predicts the $\gamma\gamma$ -decay width of 1.0×10^{-10} eV, almost seven orders smaller than the width corresponding to the single γ decay. This may be considered as an upper limit of the $\gamma\gamma/\gamma$ branching ratio since the calculated width of the γ decay, 3.5×10^{-3} eV, is smaller than the experimental data [28].

IV. SUMMARY AND CONCLUSION

Starting from Skyrme mean-field calculations we have studied for the first time the $\gamma\gamma/\gamma$ decay of the 2_1^+ state of an even-even nucleus. As our test case we considered ^{48}Ca for which its dipole polarizability has recently been measured. It can be compared also to the generalized dipole polarizability. We use the Skyrme EDF SLy5 to create a single-particle spectrum and to analyze excited states of ^{48}Ca . Our calculations take into account the coupling between one-, two- and three-phonon terms in the wave functions. It is shown that the $\gamma\gamma$ decay width is sensitive to the energy difference of the one-phonon doorway mode and the two-phonon structure which arises from the coupling of this doorway to the low-energy phonons. It is further correlated to the PPC strength. The maximal branching ratio of the competitive $\gamma\gamma$ -decay relative to its single γ -decay is predicted for ^{48}Ca as 3×10^{-8} . It is desirable to experimentally establish the $\gamma\gamma$ decay of a first 2^+ state of an even-even nucleus.

ACKNOWLEDGMENTS

A.P.S. and N.N.A. thank the hospitality of Institut für Kernphysik, Technische Universität Darmstadt where a part of this work was done. This work was partly supported by the bilateral Heisenberg-Landau program between Germany

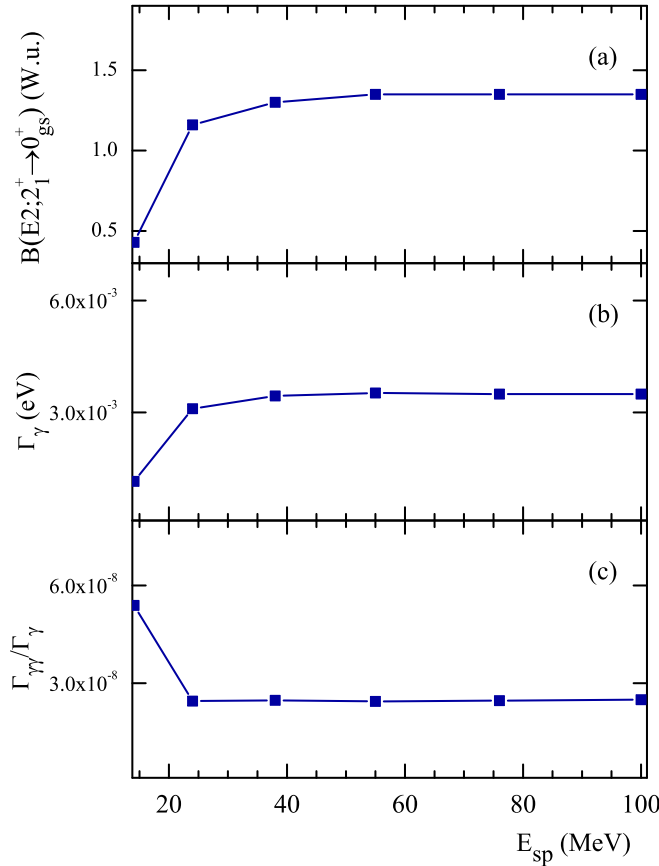


FIG. 5. The transition probability, the γ -decay width, and $\gamma\gamma/\gamma$ branching ratio of the 2_1^+ state are given in panels (a), (b), and (c), respectively. PPC3 calculations are performed with different cutoffs of single-particle energies (E_{sp}). The solid lines are drawn as guide to the eye.

and Russia, by the DFG under grant No. SFB 1245 (Project ID 279384907), and by the Cluster Project ELEMENTS supported by the State of Hesse.

APPENDIX A

The FRSA model enables one to exhaust the Thomas-Reiche-Kuhn (TRK) sum rule with the enhancement factor κ for the Skyrme EDF, i.e., $(1 + \kappa)14.8NZ/A e^2 \text{ fm}^2 \text{ MeV}$. One of the basic ingredients for the fitting protocol of the SLy5 EDF is the enhancement factor of the TRK sum rule $\kappa = 0.25$ [26], i.e., $216 e^2 \text{ fm}^2 \text{ MeV}$ in the case of ^{48}Ca . The energy-weighted sum rule of the $E1$ distribution calculated within the FRSA amounts to $210 e^2 \text{ fm}^2 \text{ MeV}$. The model configuration space depends on the cutoff of the discretized continuous part of the single-particle spectra. To confirm the two-state scenario of the α_{E1E1} calculation, one needs a maximum full configurational space. The phonon-phonon coupling calculations (PPC3) take into account the different values of single-particle energy cutoff; see Fig. 5. For the $\gamma\gamma/\gamma$ -decay branching, satisfactory convergence is reached from $E_{sp} \approx 50$ MeV. Thus, the cutoff at 100 MeV is sufficient to describe correctly the $\gamma\gamma/\gamma$ -decay branching ratio.

APPENDIX B

To calculate the dipole strength distributions, the spurious isoscalar dipole mode appears at zero excitation energy. Because of small numerical inaccuracies, the $E1$ transitions are corrected for the center-of-mass motion. The effective charges $-Z/A$ for neutrons and N/A for protons eliminate contaminations associated with the operator,

$$\hat{S} = \sum_{i=1}^A r_i Y_{1\mu}(\hat{r}_i). \quad (\text{B1})$$

To crosscheck the reliability of the prediction of α_{E1E1} , we use the orthogonalization of the spurious state to all physical states, as proposed in Ref. [36]. Starting from the wave functions (6) defined as the set $|\nu\rangle$, we construct a new set of normalized states $|\tilde{\nu}\rangle$,

$$|\tilde{\nu}\rangle = \mathcal{N}_{\tilde{\nu}}(|\nu\rangle - \eta_{\tilde{\nu}}|S\rangle), \quad (\text{B2})$$

where the state $|S\rangle$ is defined as $|S\rangle \equiv \hat{S}|0\rangle$, and $|0\rangle$ being the RPA vacuum. The set $|\tilde{\nu}\rangle$ is required to satisfy the following

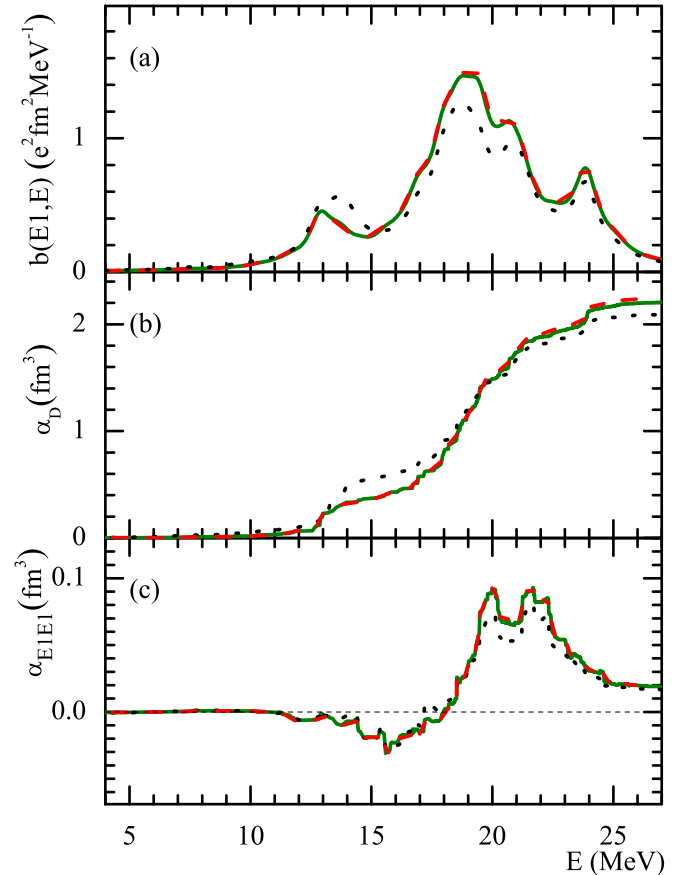


FIG. 6. (a) The $B(E1)$ strength distribution. (b) Running sum of the polarizability α_D . (c) Running sum of the generalized polarizability α_{E1E1} . The dashed line corresponds to the calculation taking into account the orthogonalization of the spurious center-of-mass state to all physical states, the dotted line is the calculation without the orthogonalization, and the solid line is the calculation with the effective charges, $e_{\text{eff}}^n = -\frac{Z}{A}e$ and $e_{\text{eff}}^p = \frac{N}{A}e$.

conditions:

$$\langle \tilde{v} | \hat{S} | 0 \rangle = 0. \quad (\text{B3})$$

As shown in Fig. 6, we found a remarkable agreement between the running sum of the generalized polarizability α_{E1E1} , obtained with the orthogonalization, and the ones, generated by means of the effective charges. Moreover, the calculation without the orthogonalization leads to very similar results for the value of α_{E1E1} . This means that the spurious center-of-mass state is well separated and it plays a minor role in our calculation of α_{E1E1} . Nevertheless, the $E1$ transitions are corrected for the center-of-mass motion.

APPENDIX C

For estimating the value of the generalized polarizability α_{M1M1} , we take the spin-flip $M1$ resonance (GR) and the initial

(2_1^+) and final (0_{gs}^+) states into account. The two-state mixing scheme then consists of the GR state, the coupled $GR \otimes 2_1^+$ state, and the interaction V between them. The model parameters are defined by means of the energy-weighted moments $m_k = \sum B(M1) E^k$: the centroid, $E_{GR} = m_1/m_0$, and the $M1$ -transition probability, $B(M1)_{GR} = m_0$. The mixed wave functions are

$$|1_{\Pi}^+\rangle = \alpha|GR\rangle + \beta|GR \otimes 2_1^+\rangle, \quad (\text{C1})$$

$$|1_{\Pi}^+\rangle = -\beta|GR\rangle + \alpha|GR \otimes 2_1^+\rangle. \quad (\text{C2})$$

The two-state model gives the following expression:

$$\alpha_{M1M1} = B(M1)_{GR} \frac{\alpha\beta\sqrt{E_{2_1^+}^2 + 4V^2}}{E_{GR}^2 - 0.25E_{2_1^+}^2 - V^2}. \quad (\text{C3})$$

-
- [1] C. Walz, H. Scheit, N. Pietralla, T. Aumann, R. Lefol, and V. Yu. Ponomarev, *Nature (London)* **526**, 406 (2015).
- [2] P.-A. Söderström, L. Capponi, E. Açıksöz, T. Otsuka, N. Tsoneva, Y. Tsunoda, D. L. Balabanski, N. Pietralla, G. L. Guardo, D. Lattuada, H. Lenske, C. Matei, D. Nichita, A. Pappalardo, and T. Petruse, *Nat. Commun.* **11**, 3242 (2020).
- [3] M. Göppert, *Über Elementarakte mit zwei Quantensprüngen*, Ph.D. thesis, Universität zu Göttingen, Germany, 1930.
- [4] J. Menéndez, A. Poves, E. Caurier, and F. Nowacki, *Nucl. Phys. A* **818**, 139 (2009).
- [5] F. Šimkovic, R. Hodák, A. Faessler, and P. Vogel, *Phys. Rev. C* **83**, 015502 (2011).
- [6] J. Barea, J. Kotila, and F. Iachello, *Phys. Rev. C* **91**, 034304 (2015).
- [7] B. A. Watson, T. T. Bardin, J. A. Becker, and T. R. Fisher, *Phys. Rev. Lett.* **35**, 1333 (1975).
- [8] A. C. Hayes, J. L. Friar, and D. Strottman, *Phys. Rev. C* **41**, 1727 (1990).
- [9] J. Schirmer, D. Habs, R. Kroth, N. Kwong, D. Schwalm, M. Zirnbaumer, and C. Broude, *Phys. Rev. Lett.* **53**, 1897 (1984).
- [10] J. Kramp, D. Habs, R. Kroth, M. Music, J. Schirmer, D. Schwalm, and C. Broude, *Nucl. Phys. A* **474**, 412 (1987).
- [11] G. Breit and E. Teller, *Astrophys. J.* **91**, 215 (1940).
- [12] D. P. Grechukhin, *Nucl. Phys.* **47**, 273 (1963).
- [13] J. Piekarewicz, B. K. Agrawal, G. Colò, W. Nazarewicz, N. Paar, P.-G. Reinhard, X. Roca-Maza, and D. Vretenar, *Phys. Rev. C* **85**, 041302(R) (2012).
- [14] G. Hagen, A. Ekström, C. Forssén, G. R. Jansen, W. Nazarewicz, T. Papenbrock, K. A. Wendt, S. Bacca, N. Barnea, B. Carlsson, C. Drischler, K. Hebeler, M. Hjorth-Jensen, M. Miorelli, G. Orlandini, A. Schwenk, and J. Simonis, *Nat. Phys.* **12**, 186 (2016).
- [15] X. Roca-Maza and N. Paar, *Prog. Part. Nucl. Phys.* **101**, 96 (2018).
- [16] A. Carbone, G. Colò, A. Bracco, L.-G. Cao, P. F. Bortignon, F. Camera, and O. Wieland, *Phys. Rev. C* **81**, 041301(R) (2010).
- [17] L. Trippa, G. Colò, and E. Vigezzi, *Phys. Rev. C* **77**, 061304(R) (2008).
- [18] A. Krasznahorkay, M. Fujiwara, P. van Aarle, H. Akimune, I. Daito, H. Fujimura, Y. Fujita, M. N. Harakeh, T. Inomata, J. Jänecke, S. Nakayama, A. Tamii, M. Tanaka, H. Toyokawa, W. Uijen, and M. Yosoi, *Phys. Rev. Lett.* **82**, 3216 (1999).
- [19] J. Terasaki, J. Engel, M. Bender, J. Dobaczewski, W. Nazarewicz, and M. Stoitsov, *Phys. Rev. C* **71**, 034310 (2005).
- [20] N. Van Giai, C. Stoyanov, and V. V. Voronov, *Phys. Rev. C* **57**, 1204 (1998).
- [21] A. P. Severyukhin, C. Stoyanov, V. V. Voronov, and N. Van Giai, *Phys. Rev. C* **66**, 034304 (2002).
- [22] V. G. Soloviev, *Theory of Atomic Nuclei: Quasiparticles and Phonons* (Institute of Physics, Bristol, UK, 1992).
- [23] A. P. Severyukhin, V. V. Voronov, and N. Van Giai, *Eur. Phys. J. A* **22**, 397 (2004).
- [24] V. Y. Ponomarev, C. Stoyanov, N. Tsoneva, and M. Grinberg, *Nucl. Phys. A* **635**, 470 (1998).
- [25] N. L. Iudice, V. Y. Ponomarev, C. Stoyanov, A. V. Sushkov, and V. V. Voronov, *J. Phys. G: Nucl. Part. Phys.* **39**, 043101 (2012).
- [26] E. Chabanat, P. Bonche, P. Haensel, J. Meyer, and R. Schaeffer, *Nucl. Phys. A* **635**, 231 (1998).
- [27] M. Bender, P.-H. Heenen, and P.-G. Reinhard, *Rev. Mod. Phys.* **75**, 121 (2003).
- [28] <http://www.nndc.bnl.gov/ensdf/>.
- [29] N. N. Arsenyev, A. P. Severyukhin, V. V. Voronov, and N. Van Giai, *Phys. Rev. C* **95**, 054312 (2017).
- [30] V. Derya, D. Savran, J. Endres, M. N. Harakeh, H. Hergert, J. H. Kelley, P. Papakonstantinou, N. Pietralla, V. Y. Ponomarev, R. Roth, G. Rusev, A. P. Tonchev, W. Tornow, H. J. Wörtche, and A. Zilges, *Phys. Lett. B* **730**, 288 (2014).
- [31] G. J. O'Keefe, M. N. Thompson, Y. I. Assafiri, R. E. Pywell, and K. Shoda, *Nucl. Phys. A* **469**, 239 (1987).
- [32] J. Birkhan, M. Miorelli, S. Bacca, S. Bassauer, C. A. Bertulani, G. Hagen, H. Matsubara, P. von Neumann-Cosel, T. Papenbrock, N. Pietralla, V. Y. Ponomarev, A. Richter, A. Schwenk, and A. Tamii, *Phys. Rev. Lett.* **118**, 252501 (2017).
- [33] D. Gambacurta, M. Grasso, and O. Vasseur, *Phys. Lett. B* **777**, 163 (2018).
- [34] R. F. Casten, *Nuclear Structure from a Simple Perspective* (Oxford University, Oxford, UK, 2000).
- [35] J. Birkhan, H. Matsubara, P. von Neumann-Cosel, N. Pietralla, V. Y. Ponomarev, A. Richter, A. Tamii, and J. Wambach, *Phys. Rev. C* **93**, 041302(R) (2016).
- [36] G. Colò, N. Van Giai, P. F. Bortignon, and M. R. Qualia, *Phys. Lett. B* **485**, 362 (2000).